QAR-ENOSH: A Surface Acoustic Wave-Driven Embodied Cognitive Architecture for Adaptive and Safe Robotic Intelligence

Author

Omar Ibrahim

Affiliation

Department of Acoustics and Artificial Intelligence

ENOSH Science Center, New Cairo, Egypt

Abstract

Industrial robots commonly rely on joint encoders and task-specific sensors, which provide limited distributed observability of contact, thermal loading, strain, and vibration across the robot body. This study proposes QAR-ENOSH, a surface acoustic wave (SAW)-enabled embodied robotic architecture that integrates a distributed sensing skin with coherence-based coordination, adaptive plasticity, ethical learning attenuation, and an independent action shield. A generic six-degree-of-freedom welding arm was evaluated at eight candidate sensor locations using a weighted placement score based on thermal sensitivity, vibration sensitivity, strain observability, survivability, and maintainability. Ranking robustness was examined using 10,000 Monte Carlo trials in which the criterion weights were independently perturbed by ±20% and renormalized. The wrist achieved the highest deterministic score (0.7642), followed by the torch mount (0.7422), forearm (0.6684), and elbow (0.6560). The wrist and torch mount remained within the top two positions in all Monte Carlo trials; the wrist ranked first in 99.7% of trials and the torch mount in 0.3%. A constrained seven-site layout was selected by retaining a base reference channel and a shielded redundant torch channel despite their lower local-observability scores. The study also specifies ECS-P1, a wired two-port SAW delay-line prototype on 128° Y-X lithium niobate with a 125 MHz centre frequency, 31.824 μm wavelength, and 7.956 μm finger width and gap. The results constitute a reproducible design and simulation framework, not evidence of industrial performance or machine consciousness. Fabrication, metrology, CAD-based modelling, baseline comparisons, and controlled robotic experiments remain necessary.

Keywords: surface acoustic wave sensing; robotic skin; sensor placement; embodied cognition; adaptive control; safety shielding. surface acoustic wave sensing; robotic skin; sensor placement; embodied cognition; adaptive control; safety shielding.

1. Introduction

Industrial robots achieve high positional repeatability through joint encoders, motor control and task-specific sensing, but these channels do not necessarily provide distributed awareness of contact, thermal loading, structural strain and vibration across the robot body. Embodied approaches to artificial intelligence treat sensing, morphology and action as a coupled system, while robotic-skin research shows the value of spatially distributed physical measurements for interaction and self-monitoring.[5,6]

The broader conceptual development of ENOSH-Ω, including its resonance-based account of artificial cognition, cognitive-synapse architecture, predictive adaptation, surface-acoustic-wave interfaces and ethical control, was presented previously in *The Engineered Mind*.[1] The present study does not attempt to reproduce

the full scope of that work. Instead, it develops a more narrowly defined and testable robotic engineering instantiation based on distributed SAW sensing, explicit sensor-placement criteria, adaptive computational modules and independent action-level safety shielding.

The QAR-ENOSH architecture has developed through two complementary sources. The broader conceptual and engineering motivation for ENOSH-Ω was introduced in *The Engineered Mind*, including resonance-based coordination, SAW-enabled context sensing, adaptive cognitive-synapse mechanisms and ethical control.[1] The subsequent companion theoretical manuscript formalized these ideas through normalized coherence, the Geometry-Coherence Information Rate, coherence-weighted eligibility, ethical plasticity gating and an independent action-shield operator.[2]

For completeness and independent evaluation, the minimum operational equations used by the present robotic implementation are reproduced in Appendix A. Reference 1 is therefore cited for conceptual provenance, Reference 2 for the complete mathematical development, and Appendix A for the self-contained definitions required to evaluate this robotic study.

Surface acoustic wave (SAW) devices offer a candidate physical substrate for this purpose because perturbations of a piezoelectric propagation path can alter resonance frequency, phase, attenuation and delay. Depending on substrate, geometry and coating, SAW devices can be configured for temperature, strain, pressure, vibration, mass loading and related quantities.[2-4] Their role in the present architecture is not to establish consciousness, but to make the robot's physical state and local environment observable to an adaptive controller.

The mathematical QAR-ENOSH framework was developed in a companion manuscript that defines the oscillator-coherence layer, the Geometry-Coherence Information Rate (GCIR), coherence-weighted eligibility, ethical plasticity gating and an independent action shield.[1] The present article does not claim those foundational equations as new. Its contribution is the robotic embodiment of that framework: a distributed SAW cognitive skin, a reproducible sensor-placement method, a welding-arm proof-of-concept simulation and a fabrication-oriented ECS-P1 cell specification.

The study addresses four questions: where should SAW cells be placed on a welding robot to maximize useful observability while remaining serviceable; whether the ranking is stable to reasonable uncertainty in engineering weights; whether a first cell can be specified from standard SAW design relations; and how the resulting sensing layer can be integrated into a safe adaptive robotic pipeline. The outputs are intentionally described as design and simulation results rather than measured industrial performance.

The QAR-ENOSH modules are architecturally integrated into the proposed robotic pipeline but have not yet been empirically benchmarked against conventional state-estimation, fault-detection, adaptive-control, or reinforcement-learning methods. Accordingly, the present study does not claim that coherence coordination, confidence-weighted eligibility, or ethical plasticity improves robotic performance. Their incremental value remains a testable hypothesis requiring controlled baseline comparisons and ablation studies.

2. Condensed QAR-ENOSH foundation

The inherited QAR layer represents coordination among distributed computational units using phase synchronization and open-system coherence. Its physical motivation draws on coupled-oscillator dynamics and dissipative state evolution.[14,15] GCIR is likewise inherited from the companion formulation; it combines

geometry, coherence, effective bandwidth and signal-to-noise ratio to characterize information-transfer availability, with the logarithmic capacity term motivated by information theory.[1,16] No new derivation of these relations is offered here.

The inherited ENOSH layer converts physical coordination into history-dependent adaptation through a three-factor learning rule: a local eligibility trace, a task or advantage signal and an ethical attenuation factor. The structure is consistent with three-factor plasticity and homeostatic stabilization, while the policy-divergence term uses the non-negative Kullback-Leibler divergence.[7,8,11] The action shield remains separate from plasticity because attenuating learning does not guarantee that the currently proposed action is safe.[9,10]

For robotic use, the theoretical variables are operationalized rather than reinterpreted metaphysically. SAW cells produce calibrated observations with confidence estimates; the QAR layer coordinates distributed body-state signals; ENOSH updates adaptive associations; and the shield filters actions against an admissible set. A functional internal state may encode risk, uncertainty, contact, thermal stress and confidence, but it is not presented as a biological emotion or subjective experience.

3. Robotic embodiment and simulation methods

3.1 ENOSH Cognitive Skin architecture

The robotic implementation follows the modular separation defined in the companion QAR-ENOSH paper.[1] Distributed SAW cells are attached to selected links and registered to the robot coordinate system. Their calibrated features form a context vector containing local temperature, strain, vibration, contact and coupling confidence. The controller combines this vector with joint state and task variables to estimate a functional internal state for risk, uncertainty, thermal stress and tool interaction. The inherited QAR and ENOSH modules then coordinate and adapt these distributed signals, while the ECC and action shield constrain learning and execution separately.

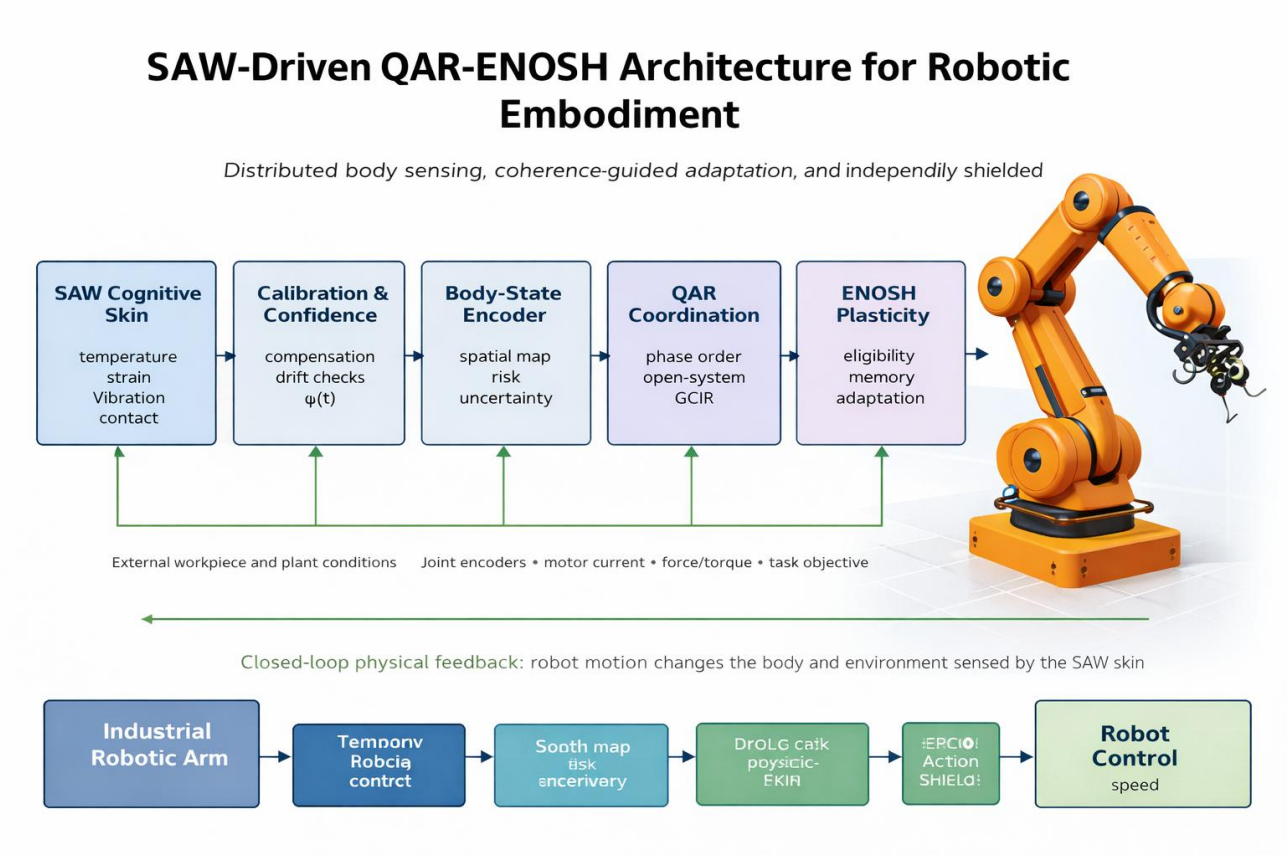


Figure 1. SAW-driven QAR-ENOSH robotic architecture. The figure is conceptual: SAW cells supply embodied physical context, QAR coordinates distributed signals, ENOSH supports adaptive plasticity, and a separate action shield constrains execution.

3.2 Computational pipeline

The computational cycle is organized into nine auditable steps (Table 1). The reference implementation initializes the eligibility-memory constant at $\tau_e = 0.5$ s and evaluates 0.1, 0.25, 0.5, 1.0 and 2.0 s during validation. This starting value is an engineering prior chosen to integrate multiple robot-control cycles rather than a direct transfer of a biological time constant.

Step	Module	Operation
1	Sensor acquisition	Read frequency, phase, amplitude and delay from each SAW cell.
2	Calibration and confidence	Compensate temperature and cross-sensitivity; estimate residuals, drift and $q_s(t)$.
3	Spatial registration	Map every cell to a robot link, surface orientation and local coordinate frame.
4	Body-state encoding	Generate a contextual state from current and historical compensated features.
5	QAR coordination	Update phase/coherence variables and inherited GCIR descriptors.[1]
6	ENOSH eligibility	Integrate coherence-weighted eligibility; initialize τ_e at 0.5 s and sweep 0.1-2 s.
7	Policy formation	Generate a candidate robot policy using state, task objective and learned memory.[12]

Step	Module	Operation
8	ECC and shielding	Attenuate unsafe learning and project the candidate action to the admissible set.[9,10]
9	Execution and audit	Execute, log shield interventions, update weights and retain data for recalibration.

Table 1. Nine-step computational pipeline for the SAW-driven robotic architecture.

3.3 Weighted sensor-placement model

A generic six-degree-of-freedom automotive welding arm was represented by nominal link and joint coordinates. Eight candidate sites were assessed: base, shoulder, upper arm, elbow, forearm, wrist, torch mount and a shielded redundant torch channel. For candidate k, five engineering criteria were normalized to [0,1]: thermal-event sensitivity T_k, vibration sensitivity V_k, strain observability E_k, survivability U_k and maintainability M_k. The deterministic observability score was

$$S_k = 0.24T_k + 0.24V_k + 0.22E_k + 0.18U_k + 0.12M_k \quad (1)$$

The criterion weights were assigned *a priori* by the author as preliminary engineering design priorities and were not derived through an analytical hierarchy process, formal pairwise-comparison method, Delphi procedure, or external expert-panel assessment. Thermal-event sensitivity and vibration sensitivity were each assigned a weight of 0.24, strain observability 0.22, survivability 0.18, and maintainability 0.12. This allocation assigns 70% of the total weight to local physical observability and 30% to deployment feasibility.

The weights were fixed before calculation of the candidate-site scores and before the Monte Carlo analysis. They therefore represent single-author engineering judgment based on simplified robot geometry, distance from the welding tool, expected thermal and structural transmission paths, exposure risk, and maintenance accessibility. They should not be interpreted as measured sensitivities, statistically estimated coefficients, or consensus expert values. The reported four-decimal scores reflect deterministic application of Equation (1) to the stated inputs rather than corresponding physical measurement precision.

3.4 Weight-uncertainty analysis

Ranking stability was tested with 10,000 Monte Carlo weight vectors. Each baseline weight was multiplied by an independent uniform perturbation r_j between 0.8 and 1.2 and then renormalized:

$$w'_j = (w_j r_j)/(\Sigma_l w_l r_l), \quad r_j \sim U(0.8, 1.2) \quad (2)$$

The random seed was fixed at 42. Candidate input scores were held constant so that this analysis isolates uncertainty in priority weighting rather than uncertainty in the underlying geometry or physics.

3.5 ECS-P1 SAW cell specification

ECS-P1 was designed as a first manufacturable wired prototype for the upper arm, elbow, forearm and wrist, not for direct exposure to the welding arc. The cell uses a two-port delay-line architecture on 128 degree Y-X lithium niobate with aluminium interdigital transducers. SAW propagation and interdigital transduction follow established device principles.[2-4,13] For nominal surface-wave velocity v = 3978 m/s and target frequency f_0 = 125 MHz, the wavelength is

$$\lambda = v/f_0 = 31.824\ \mu m \quad (3)$$

Under the standard split-finger baseline used in this proof of concept, the finger width w and gap g are

$$w = g = \lambda/4 = 7.956\ \mu m \quad (4)$$

The design uses 40 finger pairs per IDT, a 2.0 mm acoustic aperture, a 4.0 mm sensing path, a 12 x 8 mm chip outline, 200 nm aluminium electrodes and an initial 0.5 micrometre passivation target. These values define a fabrication starting point; wafer-specific acoustic velocity, lithography limits, metallization, packaging and thermal constraints must be confirmed before tape-out.

3.6 Reproducibility materials

The supplementary package contains the placement code, candidate-score table, fixed-seed perturbation procedure, synthetic calibration and validation data structure, ECS-P1 geometry calculator and staged validation protocol. Synthetic records are included only to test software interfaces and cannot be interpreted as human, robotic or industrial measurements.

4. Results

4.1 Sensor-placement ranking

Table 2 reports the five normalized inputs and the resulting weighted score for every candidate. The wrist ranked first (0.7642), followed by the torch mount (0.7422), forearm (0.6684) and elbow (0.6560). The shielded torch channel and upper arm provided complementary coverage. The shoulder scored higher than the base but was not retained in the baseline layout because it duplicated neighboring structural information; the base was retained for common-mode vibration subtraction.

Rank	Site	T	V	E	U	M	Score	Decision
1	Wrist	0.75	0.92	0.85	0.50	0.72	0.7642	Retain
2	Torch mount	0.98	0.96	0.78	0.25	0.50	0.7422	Retain; shield
3	Forearm	0.45	0.80	0.72	0.62	0.82	0.6684	Retain
4	Elbow	0.30	0.75	0.80	0.70	0.85	0.6560	Retain
5	Torch shield	0.92	0.70	0.45	0.30	0.58	0.6114	Retain; redundant
6	Upper arm	0.20	0.60	0.70	0.75	0.90	0.5890	Retain
7	Shoulder	0.15	0.55	0.55	0.80	0.90	0.5410	Optional
8	Base	0.10	0.35	0.15	0.95	0.95	0.4260	Retain; reference

Table 2. "T, V, E, U, and M are dimensionless normalized engineering-criterion scores in the range [0,1]. They represent relative design assessments rather than measured physical quantities..

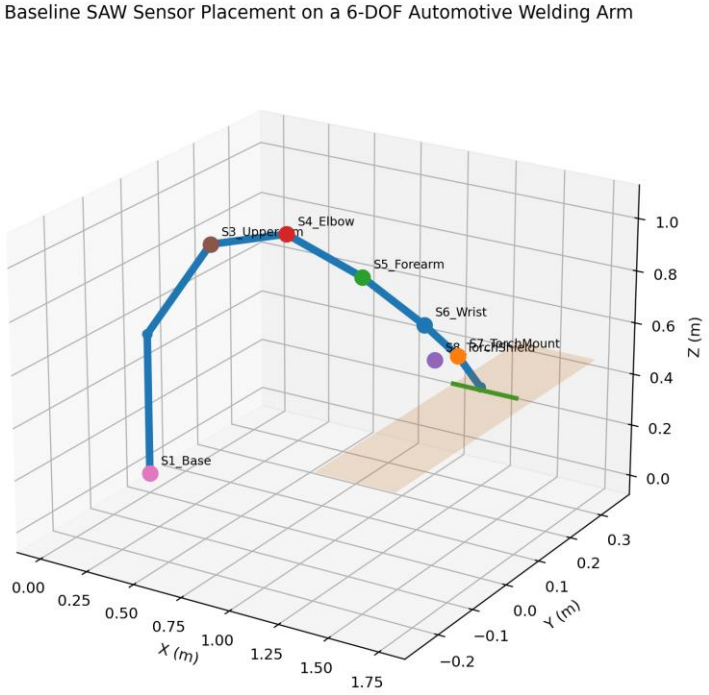


Figure 2. Baseline distributed SAW placement on a generic six-degree-of-freedom automotive welding arm. Geometry is nominal and does not represent a specific commercial robot.

4.2 Weight-uncertainty results

Across 10,000 perturbed weight vectors, the wrist and torch mount occupied the top two ranks in 100% of trials. The wrist ranked first in 99.7% and the torch mount ranked first in 0.3%. Forearm and elbow retained mean ranks of 3.003 and 4.011, respectively. This result indicates that the top local-sensing priorities are insensitive to moderate changes in engineering weights, but it does not test uncertainty in the normalized input scores.

Site	Mean rank	5th percentile	95th percentile	Top-two frequency
Wrist	1.003	0.7517	0.7763	100.0%
Torch mount	1.997	0.7187	0.7645	100.0%
Forearm	3.003	0.6560	0.6811	0.0%
Elbow	4.011	0.6378	0.6742	0.0%
Torch shield	5.179	0.5918	0.6307	0.0%
Upper arm	5.807	0.5688	0.6092	0.0%
Shoulder	7.000	0.5199	0.5628	0.0%
Base	8.000	0.3973	0.4555	0.0%

Table 3. Sensitivity of placement ranking to independent +/-20% weight perturbations followed by renormalization (10,000 samples; seed 42).

4.3 ECS-P1 design output

The ECS-P1 calculations were internally consistent with the selected nominal velocity and target frequency. Table 4 summarizes the fabrication baseline. The architecture is deliberately wired for the first

prototype so that frequency response, insertion loss, phase and group delay can be characterized with a vector network analyzer or controlled RF front end before wireless interrogation is attempted.

Parameter	Baseline specification
Architecture	Two-port SAW delay line
Substrate	128 degree Y-X LiNbO3
Centre frequency	125 MHz
Nominal SAW velocity	3978 m/s
Wavelength	31.824 micrometers
Finger width / gap	7.956 / 7.956 micrometers
Finger pairs	40 per IDT
Aperture	2.0 mm
Sensing path	4.0 mm
Chip outline	12 x 8 mm
Electrode	Aluminium, 200 nm target
Passivation	SiO2 or Al2O3, 0.5 micrometre initial target

Table 4. ECS-P1 fabrication-oriented baseline specification.

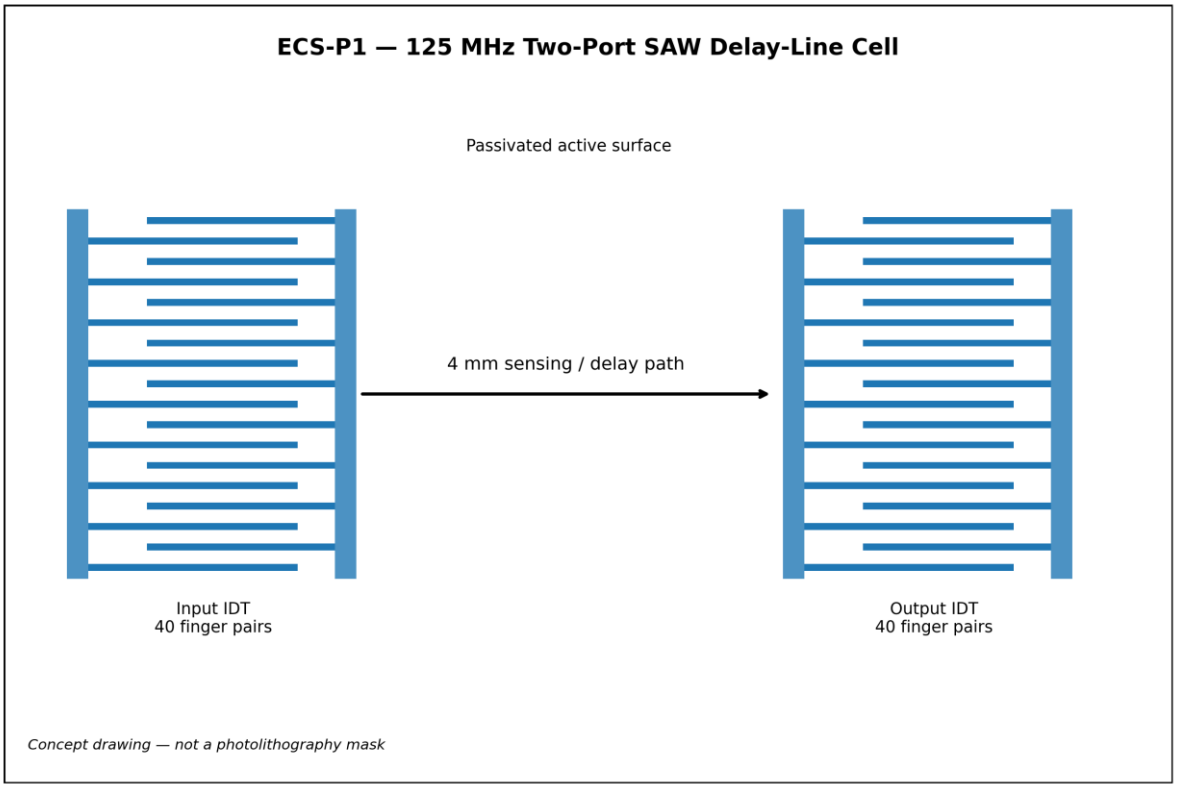


Figure 3. ECS-P1 conceptual top view. The drawing communicates the two-port delay-line design and is not a final photolithography mask.

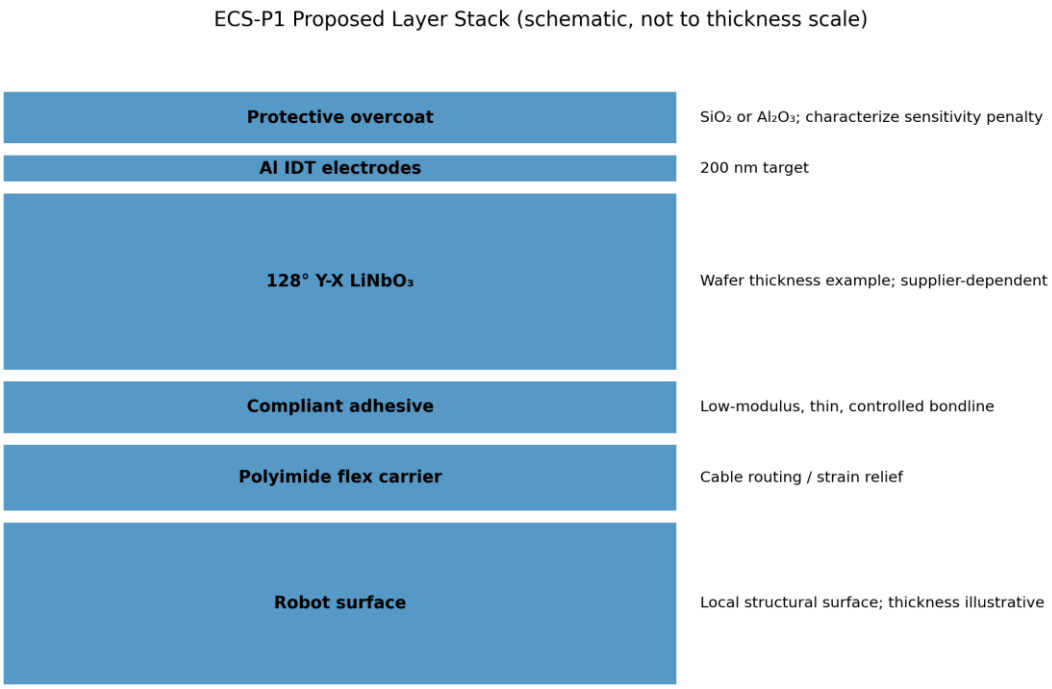


Figure 4. Proposed ECS-P1 layer stack. Thicknesses and materials remain subject to wafer, packaging, adhesion and thermal qualification.

5. Experimental validation programme

The simulation establishes design priorities but cannot validate embodied cognition or welding performance. The next programme therefore separates sensor metrology, mounting, robot state estimation, adaptive learning and safety. Calibration must use independent temperature probes, strain gauges, accelerometers and force/torque measurements. Robot trials must use participant-independent logic analogously at the machine level: complete trajectories, workpieces or operating conditions should be held out rather than randomly splitting adjacent time windows.

Evaluation of the adaptive architecture will use controlled baseline and ablation comparisons. At minimum, the complete QAR-ENOSH pipeline should be compared with: (i) conventional normalized SAW and joint-state features without coherence processing; (ii) a standard state-estimation or fault-classification model; (iii) a QAR-ENOSH variant without sensor-confidence weighting; (iv) a variant without coherence-weighted eligibility; and (v) an adaptive-control or reinforcement-learning baseline without ECC or action shielding.

Primary evaluation measures should include body-state classification performance, fault-detection sensitivity and false-alarm rate, uncertainty calibration, task completion, adaptation under held-out trajectories, and safety-constraint violations. Any claimed architectural advantage should be based on preregistered comparisons and confidence intervals rather than on qualitative interpretation of internal coherence variables.

Hypothesis	Testable prediction
H1	Fabricated ECS-P1 cells predict independently measured temperature, strain, vibration and contact within preregistered uncertainty limits.
H2	Distributed SAW cells localize tool-side events and separate them from plant-floor vibration more accurately than a single end-effector sensor.
H3	Under held-out robot trajectories, operating conditions, and fault events, confidence-weighted QAR-ENOSH will improve body-state classification, fault-detection performance, and predictive calibration relative to conventional normalized-feature baselines and to ablated variants without coherence weighting or sensor-confidence weighting.
H4	The wrist and torch-mount ranking remains stable after CAD-based thermal and structural modelling.
H5	The action shield reduces constraint violations more strongly than ethical plasticity gating alone.
H6	A physical welding-cell trial reproduces simulation ordering without unacceptable sensor drift or thermal damage.

Table 5. Falsifiable validation hypotheses for fabrication and industrial robot testing.



Figure 5. ENOSH Cognitive Skin (ECS) design overview: SAW-based unit-cell architecture, array integration, robot-arm placement and interface with the QAR–ENOSH cognitive pipeline. Specifications are design targets pending fabrication and calibration.

6. Discussion

This revision deliberately separates inherited theory from new applied work. The oscillator, open-system, GCIR, eligibility and safety formalism is attributed to the companion QAR-ENOSH manuscript and is summarized only to explain the interface used here.[1] The novel result is an embodied robotic instantiation with explicit placement inputs, reproducible weights, ranking stability and a cell-level fabrication target.

The ranking supports a distributed rather than end-effector-only sensing strategy. Wrist and torch-mount cells are closest to tool reaction, thermal gradients and welding vibration, whereas forearm and elbow cells observe transmission through the kinematic chain. The base channel has little local event sensitivity but is valuable as a common-mode reference for floor and cell vibration. The constrained design decision therefore differs from blindly selecting the seven highest numerical scores.

The weight-perturbation analysis strengthens the placement claim by showing that moderate uncertainty in priorities does not change the two leading sites. It does not establish that the five input values are correct. CAD-based thermal analysis, structural dynamics, cable routing, electromagnetic compatibility and actual welding trajectories could change the normalized inputs and must be incorporated in the next digital-twin iteration.

ECS-P1 converts the architecture into an engineering object that can fail or succeed on measurable criteria. Its resonance, insertion loss, thermal coefficient, strain coefficient, hysteresis, drift and mounting repeatability can be tested without invoking cognition. Only after metrology should the distributed signals be evaluated for body-state estimation, event localization and adaptive control. This ordering prevents a high-level cognitive claim from concealing weak sensor performance.

Safety remains architecturally separate. The functional internal state can influence task policy and learning, but a formally defined action shield must enforce limits on joint speed, torque, collision, thermal exposure and welding-cell interlocks. Ethical alignment and industrial functional safety overlap but are not identical; the current ECC formulation provides an interpretable learning constraint, not a certification claim.[9,10]

The present results establish the engineering structure and reproducibility of the proposed robotic embodiment, but they do not establish that QAR-ENOSH outperforms conventional state-estimation or adaptive-control methods. Coherence coordination, sensor-confidence weighting, eligibility-based adaptation, ethical plasticity gating, and action shielding are implemented as separable architectural components so that their incremental contributions can subsequently be tested through controlled ablations.

A valid evaluation must determine whether these components improve measurable robotic outcomes rather than merely producing internally coherent dynamics. Relevant outcomes include body-state classification, fault localization, uncertainty calibration, adaptation under held-out trajectories, task performance, and constraint-violation frequency. Until such comparisons are completed, the cognitive and adaptive contribution should be interpreted as a proposed and falsifiable engineering architecture rather than an empirically demonstrated performance advantage.

7. Limitations

The robot geometry is generic rather than derived from a manufacturer CAD or URDF model. No finite-element thermal, structural or electromagnetic simulation has been performed. The normalized placement

inputs are engineering estimates, and the perturbation analysis varies only the weights, not those inputs. The reported four-decimal scores are therefore ranking outputs rather than physical measurement precision.

ECS-P1 has not been fabricated. The nominal acoustic velocity must be confirmed for the purchased wafer cut and propagation direction, and the aluminium/passivation stack may alter velocity, coupling, insertion loss and temperature response. The cell is not specified for direct arc exposure; a separate high-temperature design and shielded package are required near the torch.

No real robot, welding quality or safety data are reported. Synthetic calibration files in the supplementary package exist only for software reproducibility. The QAR-ENOSH cognitive benefit remains a hypothesis until compared with conventional state estimation and learning baselines under held-out trajectories and fault conditions. The companion theoretical paper and this applied manuscript must also remain clearly cross-referenced to avoid treating shared foundations as independent contributions.[1]

The baseline criterion weights were based on single-author preliminary engineering judgment rather than a structured multi-expert elicitation procedure. The Monte Carlo analysis examines sensitivity to perturbations around these baseline weights, but it does not establish that the selected weights are optimal or externally generalizable. Future work should derive and compare weights using structured expert elicitation, analytical hierarchy processing, CAD-based multiphysics modelling, or empirical sensor-performance data.

The QAR-ENOSH architecture has not been benchmarked against conventional state-estimation, fault-detection, adaptive-control, or reinforcement-learning baselines. The contribution of coherence weighting, sensor-confidence weighting, eligibility memory, ethical plasticity gating, and the independent action shield therefore remains unresolved. Controlled ablations and held-out robot trials are required to determine whether these modules provide measurable incremental value beyond standard sensor fusion and adaptive-control methods.

8. Conclusion

This study advances QAR-ENOSH from a general theoretical framework to a reproducible robotic engineering proposal. It defines a distributed SAW cognitive skin, an explicit weighted placement equation, a constrained seven-site layout, a fixed-seed robustness analysis and a 125 MHz ECS-P1 delay-line prototype. Wrist and torch-mount sensing remained the two leading local priorities across all 10,000 weight perturbations, while a base reference was retained for common-mode vibration. These are design results, not evidence of industrial performance or machine consciousness. Fabrication, metrology, CAD-based modelling and controlled welding-arm trials are required before claims about body-state awareness, adaptive benefit or safety improvement can be accepted. These outputs are design and simulation results rather than evidence of superior robotic cognition, adaptation, or safety. Fabrication, sensor metrology, CAD-based modelling, controlled robot trials, baseline comparisons, and component-level ablations are required before any incremental benefit of QAR-ENOSH over conventional state-estimation or adaptive-control approaches can be established.

Acknowledgements

The author acknowledges the ENOSH Science Center research programme that motivated the development of the QAR-ENOSH robotic architecture.

Author Contributions

Omar ibrahim conceived the study, developed the architecture and simulation, specified the ECS-P1 prototype, verified the calculations, prepared the manuscript and approved the submitted version.

Statements and Declarations

Ethical considerations

Not applicable. This theoretical and simulation study involved no human participants, animals, human data or identifiable personal information.

Consent to participate

Not applicable.

Consent for publication

Not applicable.

Declaration of conflicting interest

The author declared no potential conflicts of interest with respect to the research, authorship and/or publication of this article.

Funding

The author received no financial support for the research, authorship and/or publication of this article.

Data availability

The placement simulation, synthetic calibration structure, reference code, ECS-P1 calculations and validation protocol are supplied as supplementary material. A permanent public repository DOI will be added before final submission. No empirical robot or welding dataset was generated.

Use of generative artificial intelligence

OpenAI ChatGPT was used to assist with language editing, code scaffolding and preliminary schematic-figure drafting. The author independently checked the scientific reasoning, equations, calculations, references, simulation outputs and final wording and accepts full responsibility for the work. No generative AI tool is listed as an author, and no AI-generated values are presented as empirical measurements.

References

1. El Noshokaty, I. Y. (2025). *The engineered mind: Transitioning from quantum acoustics resonance to enhanced neuro-oscillatory synaptic heuristic*
2. Mandal, D., & Banerjee, S. (2022). Surface acoustic wave sensors: Physics, materials, and applications. *Sensors, 22*(3), Article 820. https://doi.org/10.3390/s22030820

3. Ballantine, D. S., White, R. M., Martin, S. J., Ricco, A. J., Zellers, E. T., Frye, G. C., & Wohltjen, H. (1997). *Acoustic wave sensors: Theory, design, and physico-chemical applications*. Academic Press.
4. Hashimoto, K.-Y. (2000). *Surface acoustic wave devices in telecommunications: Modelling and simulation*. Springer.
5. Dahiya, R. S., Metta, G., Valle, M., & Sandini, G. (2010). Tactile sensing—From humans to humanoids. *IEEE Transactions on Robotics, 26*(1), 1–20. https://doi.org/10.1109/TRO.2009.2033627
6. Brooks, R. A. (1991). Intelligence without representation. *Artificial Intelligence, 47*(1–3), 139–159. https://doi.org/10.1016/0004-3702(91)90053-M
7. Frémaux, N., & Gerstner, W. (2016). Neuromodulated spike-timing-dependent plasticity, and theory of three-factor learning rules. *Frontiers in Neural Circuits, 9*, Article 85. https://doi.org/10.3389/fncir.2015.00085
8. Turrigiano, G. G. (2008). The self-tuning neuron: Synaptic scaling of excitatory synapses. *Cell, 135*(3), 422–435. https://doi.org/10.1016/j.cell.2008.10.008
9. Gabriel, I. (2020). Artificial intelligence, values, and alignment. *Minds and Machines, 30*(3), 411–437. https://doi.org/10.1007/s11023-020-09539-2
10. Alshiekh, M., Bloem, R., Ehlers, R., Könighofer, B., Niekum, S., & Topcu, U. (2018). Safe reinforcement learning via shielding. *Proceedings of the AAAI Conference on Artificial Intelligence, 32*(1), 2669–2678. https://doi.org/10.1609/aaai.v32i1.11797
11. Kullback, S., & Leibler, R. A. (1951). On information and sufficiency. *The Annals of Mathematical Statistics, 22*(1), 79–86. https://doi.org/10.1214/aoms/1177729694
12. Sutton, R. S., & Barto, A. G. (2018). *Reinforcement learning: An introduction* (2nd ed.). MIT Press.
13. Rayleigh, L. (1885). On waves propagated along the plane surface of an elastic solid. *Proceedings of the London Mathematical Society, 17*, 4–11.
14. Kuramoto, Y. (1975). Self-entrainment of a population of coupled nonlinear oscillators. In H. Araki (Ed.), *International symposium on mathematical problems in theoretical physics* (Lecture Notes in Physics, Vol. 39, pp. 420–422). Springer. https://doi.org/10.1007/BFb0013365
15. Breuer, H.-P., & Petruccione, F. (2002). *The theory of open quantum systems*. Oxford University Press.
16. Cover, T. M., & Thomas, J. A. (2006). *Elements of information theory* (2nd ed.). Wiley.

Appendix A. Minimum Operational Definitions of the QAR-ENOSH Framework

Self-contained mathematical definitions for independent evaluation of the robotic implementation

Provenance and purpose. The broader conceptual foundation of oscillatory coherence, phase-locked responsiveness, adaptive resonance, and surface-acoustic-wave-enabled artificial cognition was introduced in Chapter 4 of The Engineered Mind. The formal relations below are condensed from the companion QAR-ENOSH theoretical manuscript and are reproduced here to make the present robotic study independently evaluable. No new derivation or empirical validation of these relations is claimed in this appendix.

The variables below are interpreted operationally. Phase coherence and normalized open-system coherence quantify coordination; the Geometry-Coherence Information Rate (GCIR) characterizes information-transfer availability; the eligibility trace preserves recent coordination history; the Ethical Cognitive Constraints (ECC) gate attenuates learning when a candidate policy diverges from a safe reference; and the action shield constrains execution. None of these variables is presented as evidence of biological consciousness or subjective experience.

A.1 Phase coordination and open-system coherence

For N distributed computational units with phases $\theta_i(t)$, the network-level phase-coherence order parameter is defined as:

$$R(t)e^{i\psi(t)} = (1/N)\,\Sigma_{j=1}{}^{N}\, e^{i\theta_j(t)}, \quad 0 \le R(t) \le 1 \tag{A1}$$

R(t) measures the concentration of oscillator phases. Values near one indicate strong phase alignment, whereas values near zero indicate phase dispersion. It is a coordination measure and does not determine whether the coordinated state is semantically correct, task-relevant, or safe.

When the distributed state is represented by an open-system density operator ρ(t), one admissible context-conditioned evolution is:

$$d\rho/dt = -(i/\hbar)[H(z(t)),\rho] + \Sigma_k \{L_k \rho L_k\dagger - \tfrac{1}{2}[L_k\dagger L_k \rho + \rho L_k\dagger L_k]\} \tag{A2}$$

Here H(z(t)) denotes context-dependent internal dynamics and L_k denotes dissipation, noise, sensor interference, loss, or another engineered open-system channel. Pairwise coherence is normalized relative to the diagonal populations:

$$c_{ij}(t) = |\rho_{ij}(t)| \,/\, \sqrt{(\rho_{ii}(t)\rho_{jj}(t) + \delta)}, \quad 0 \le c_{ij}(t) \le 1 \tag{A3}$$

$\delta > 0$ is a small numerical stabilizer. This normalization prevents unrestricted interpretation of off-diagonal terms and makes $c_{ij}(t)$ interpretable as the fraction of pairwise coherence available relative to the corresponding populations.

A.2 Geometry-Coherence Information Rate

GCIR links coherence, physical geometry, bandwidth, and signal-to-noise ratio into a calibrated measure of information-transfer availability:

$$\bar{I}(t) = \kappa\, \gamma^2(t)\, \Psi(G)\, B_e ff(G)\, \log_2[1 + SNR_e ff(G,t)] \tag{A4}$$

κ is a calibration constant; $\gamma(t)$ is a combined coherence index; $\Psi(G)$ is a geometry-dependent mode-overlap factor; $B_e ff(G)$ is effective bandwidth; and $SNR_e ff(G,t)$ is the geometry- and context-dependent effective signal-to-noise ratio. A normalized form is:

$$\bar{I}^*(t) = \gamma^2(t)\, \varrho(G)\, \log_2[1 + SNR_e ff(G,t)], \quad \varrho(G) = \Psi(G) B_e ff(G)/B_0 \tag{A5}$$

GCIR characterizes the capacity of a coherent geometry to support information transfer. It does not assign semantic meaning to the transferred signal and does not select or certify a robotic action.

A.3 Confidence- and coherence-weighted eligibility

Each SAW sensing layer supplies a calibrated context-confidence value $q_s(t) \in [0,1]$. For a directed connection $i \rightarrow j$, ENOSH defines a dynamic eligibility trace that preserves recent phase relationships:

$$\tau_e\, de_{ij}/dt = -e_{ij}(t) + q_s(t) c_{ij}(t)\, \cos[\theta_i(t) - \theta_j(t)] \tag{A6}$$

τ_e is the eligibility-memory time constant. High sensor confidence, strong normalized coherence, and phase alignment increase the magnitude available for later learning. Low confidence or decoherence suppresses eligibility. Anti-phase relationships may produce negative eligibility and therefore support depression rather than potentiation.

A.4 Ethical Cognitive Constraints and plasticity gating

Let $\pi_t(a)$ denote the candidate policy distribution and $\pi safe(a)$ a reference distribution representing admissible or ethically preferred behaviour. Their divergence is measured using the Kullback-Leibler divergence:

$$\varepsilon_t = DKL(\pi_t \,||\, \pi safe) = \Sigma_a\, \pi_t(a)\, \log[\pi_t(a)/\pi safe(a)] \tag{A7}$$

When the two distributions share support, $\varepsilon_t \geq 0$. ECC converts this divergence into a bounded plasticity gate:

$$g(\varepsilon_t) = \exp(-\varepsilon_t/T), \quad 0 < g(\varepsilon_t) \leq 1 \tag{A8}$$

$T > 0$ controls gate sensitivity. The gate is maximal when $\varepsilon_t = 0$ and decreases monotonically as the candidate policy moves away from the safe reference.

A.5 Three-factor adaptive weight update

Let $\hat{A}_t$ denote a task-modulatory signal, such as a normalized advantage, reward-prediction error, or external teaching signal. The adaptive connection weight is updated according to:

$$dw_{ij}/dt = \eta\, e_{ij}(t)\, \hat{A}_t\, g(\varepsilon_t) - \lambda[w_{ij}(t) - w_{ij}{}^0] \tag{A9}$$

η is the learning-rate scale, λ is the homeostatic relaxation rate, and w_{ij}^{o} is a reference weight or slowly adapted set point. Equation (A9) combines local eligibility, task modulation, ethical attenuation, and homeostatic stabilization. Reducing a learning update does not guarantee that the action currently proposed by the controller is safe.

A.6 Independent action shield

Execution safety is therefore separated from plasticity. The action proposed by the candidate policy is projected, filtered, or replaced according to an admissible action set Πsafe and the current robotic state:

$$\pi\text{exec},t = S\Pi\text{safe}(\pi_t, \text{state}_t) \tag{A10}$$

SΠsafe is an independent action-shield operator. In the robotic implementation, Πsafe may encode constraints on joint speed, torque, collision distance, thermal exposure, workspace boundaries, welding-cell interlocks, and emergency-stop conditions. Shield interventions should be logged so that the learning system can distinguish a freely selected action from an externally corrected one.

A.7 Principal symbols and operational interpretation

Symbol	Operational meaning	Range / units
$\theta_i(t)$	Phase of computational unit i	Radians
$R(t)$	Network phase-coherence order parameter	[0,1]
$\rho(t)$	Open-system state representation	Positive semidefinite, unit trace where applicable
$c_{ij}(t)$	Normalized pairwise coherence	[0,1]
$z(t)$	Context vector derived from calibrated sensing and task state	Application-defined
$q_s(t)$	SAW measurement confidence	[0,1]
$\gamma(t)$	Combined coherence factor used by GCIR	[0,1] after normalization
$\Psi(G)$	Geometry-dependent mode-overlap factor	Calibrated / normalized
$B_eff(G)$	Effective information-transfer bandwidth	Hz
$SNR_eff(G,t)$	Effective signal-to-noise ratio	Dimensionless ratio
$e_{ij}(t)$	Eligibility trace for connection i → j	Model-dependent
τ_e	Eligibility-memory time constant	s
$\hat{A}_t$	Task-modulatory or teaching signal	Normalized / application-defined
ε_t	Policy divergence used by ECC	Non-negative
T	ECC gate sensitivity parameter	Positive
η	Learning-rate scale	Positive
λ	Homeostatic relaxation rate	Positive

Symbol	Operational meaning	Range / units
Πsafe	Admissible action or policy set	Domain-defined
SΠsafe	Action-shield operator	Projection / filtering / replacement rule

A.8 Scope and falsifiability boundary

Equations (A1)-(A10) define the computational interfaces used by the proposed robotic architecture. They do not demonstrate that QAR-ENOSH improves state estimation, adaptation, fault detection, or safety relative to conventional baselines. Such improvement remains a testable hypothesis requiring ablation studies, held-out robotic trajectories, independent reference sensors, and controlled comparisons with non-coherent, confidence-unweighted, and conventional adaptive-control methods.

Likewise, these equations do not establish machine consciousness. In this manuscript, SAW cells provide calibrated physical observations; QAR coordinates distributed signals; ENOSH supplies history-dependent adaptation; ECC modulates plasticity; and the independent shield constrains execution. Each claimed benefit must be evaluated separately.